NANO LETTERS

pubs.acs.org/NanoLett Letter

Tuning the Intrinsic Stochasticity of Resistive Switching in VO_2 Microresistors

Noémie Bidoul,* Nicolas Roisin, and Denis Flandre*

Cite This: *Nano Lett.* 2024, 24, 6201−6209 Read Online

ACCESS | Metrics & More | Article Recommendations | Supporting Information

ABSTRACT: Vanadium dioxide (VO_2) microresistors exhibit resistive switching above a certain threshold voltage, allowing them to emulate neurons in neuromorphic systems. However, such devices present intrinsic cycle-to-cycle variations in their resistances and threshold voltages, which can be detrimental or beneficial, depending on their use. Here, we study this stochasticity in VO_2 microresistors with various grain sizes and dimensions, through high-resolution electrical and optical measurements across numerous cycles. Our results highlight that the cycle-to-cycle variations in threshold voltage increase as the grain size becomes comparable to the device dimensions. We also present observations of multimodal threshold voltage distributions in the smaller-length resistors. To understand the underlying phenomenon, we investigate the relationship between the device insulating resistance and threshold voltage distributions, showing that these modes could correspond to distinct percolation paths and filaments. Our findings provide the first experimentally verified guidelines for designing VO_2 devices with minimized/maximized stochasticity, depending on the targeted application.

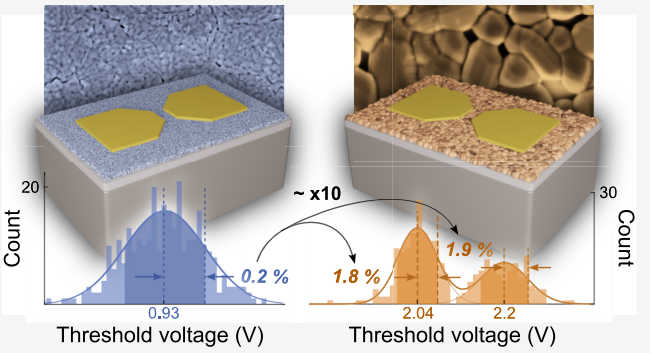

KEYWORDS: *resistive switching, stochasticity, cycle-to-cycle variations, insulator-to-metal transition, grain size, device dimensions*

Vanadium dioxide is a material that undergoes an insulator-to-metal transition (IMT) from an insulating state with a monoclinic crystalline structure to a conductive state with a rutile crystalline structure upon increased temperature. This transition is accompanied by a reduction in resistivity of several orders of magnitude. In VO_2 two-terminal microresistors, the transition can also be triggered by the application of an external voltage, through a debated combination of thermal effects (Joule heating) and electrical effects (critical carrier density).[1−3] This volatile and hysteretic transition takes place through a filamentary process,[4−6] meaning only a portion of the device becomes metallic. Figure 1 shows a typical VO_2 microresistor along with its hysteretic $I-V$ characteristic and optical imaging of the metallic filament. This phenomenon is of particular interest in neuromorphic systems and has been harnessed to emulate analog spiking neurons, both computational[7−10] and sensory.[11−18] These neurons could respectively serve as functional units and entry layers for spiking neural networks, enabling sparse and energy-efficient encoding of information.[19,20]. On the other hand, memristive effects attributed to nonvolatile film alterations have been put in evidence in VO_2 microresistors,[21−25] opening the possibility to use them to emulate synapses.

All of these promising applications must deal with a specificity of VO_2 two-terminal devices: the variations of their electrical characteristics from cycle to cycle. These characteristics—depicted in Figure 1b—include the device insulator-to-metal and metal-to-insulator threshold voltages V_{IMT} and V_{MIT}, respectively, its voltage-dependent resistance in the insulating state ($R_{ins,0}$ close to zero bias and R_{IMT} close to the transition), and its resistance in the metallic state R_{met}. In certain applications of VO_2 microresistors, such cycle-to-cycle variations are desired and have been harnessed to realize stochastic functions including probabilistic bits,[26−28] neurons implementing stochastic phase-locked firing or skipping[7] and stochastic resonance,[29] stochastic oscillators,[30,31] and random access memories.[32] In other cases, e.g. in sensory VO_2 neurons where stimuli are encoded in the spike rate,[11−16] these variations should be minimized as they induce jitter on the oscillator frequency and can thus impede the sensor resolution, as shown in a previous work.[12] However, so far, there exist no guidelines to design VO_2 microresistors with controlled stochasticity, meaning their functionality will be impeded by the microfabricated film's intrinsic physical properties.

Although the mechanisms behind these variations are not fully understood, two phenomena stand out as possible causes,

Received: January 12, 2024
Revised: May 16, 2024
Accepted: May 16, 2024
Published: May 17, 2024

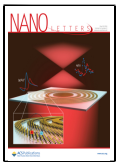

https://doi.org/10.1021/acs.nanolett.4c00184
Nano Lett. 2024, 24, 6201−6209

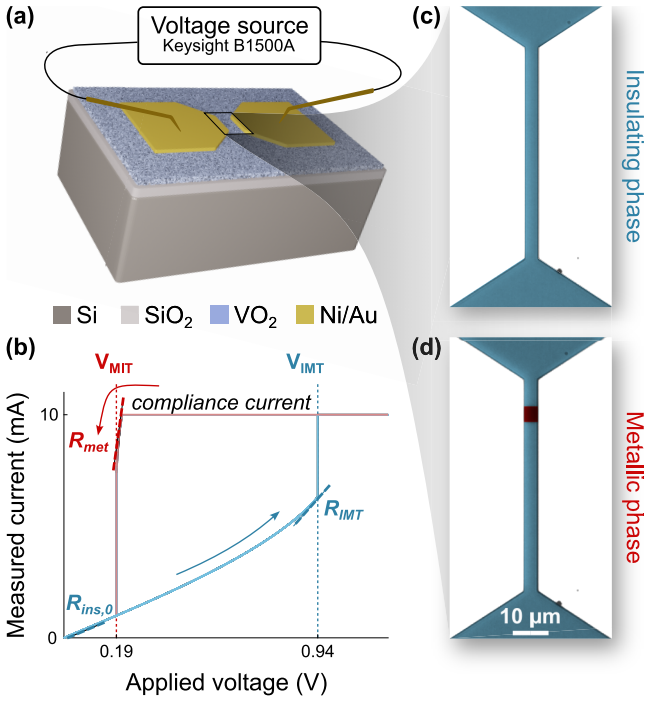

Figure 1. (a) Structure of a typical VO_2 two-terminal device, together with the measurement setup used to extract its $I-V$ characteristic. (b) Hysteretic voltage-driven $I-V$ characteristic of a VO_2 two-terminal device, together with its electrical parameters in the insulating (blue) and metallic (red) regimes. These parameters are the device insulator-to-metal and metal-to-insulator threshold voltages V_{IMT} and V_{MIT}, respectively, its voltage-dependent resistance in the insulating state ($R_{ins,0}$ close to zero bias, and R_{IMT} close to the transition), and its resistance in the metallic state R_{met}. Resistances were extracted through linear regression around a bias point. A current compliance is set on the voltage source to protect the device in its metallic regime. (c,d) High-resolution microscopy images of a VO_2 two-terminal device in both regimes. In its low resistance state (d), the metallic filament is visible through contrast thanks to the change of optical constants of the VO_2 film when transitioning. Blue (insulating) and red (metallic) colors have been added to the plot to enhance the distinction between the two phases.

both of which take place during the relaxation from metal to insulator (MIT). A first possible mechanism is the presence of long-lived metallic domains[25,35−37] which can persist up to several milliseconds after the metallic filament resorption (once the applied voltage is removed), in the region of the device where the filament previously formed. Indeed, these metallic islands serve as preferential nucleation sites for the next transition,[37] and their expected random nature[27] could result in slightly different insulating resistances and threshold voltages from cycle to cycle. The presence of these metallic domains has been observed through nano-XRD,[25] optical reflectivity,[35] and dark-field X-ray microscopy measurements.[37] A second possible mechanism is the fact that individual grains might change crystalline orientation from cycle to cycle, impacting the device insulating resistance and threshold voltage. These changes have been imaged through TEM,[38] and four possible transition pathways have been computed for a crystallite undergoing MIT, corresponding to four 90°-symmetrical crystalline orientations of the insulating phase. Stochasticity could also be due to a combination of these two phenomena. In both observations, variations of properties in individual grains are involved: one thus expects to witness a larger impact on the microresistor electrical property variations as device dimensions get closer to crystallite size. However, such a claim[38] has never been experimentally verified nor the impact on the magnitude of stochasticity quantified: this will be the focus of this work. To test whether stochasticity is dependent on the grain size/device dimensions ratio, we will successively study the impact of grain size and VO_2 microresistor length.

Starting with grain size, we synthesized two types of VO_2 thin films of identical 135 nm thickness, but a 10-fold difference in grain size. Both films were deposited on silicon substrates with a 200 nm thick wet thermal SiO_2 layer, at room temperature through reactive DC sputtering from a vanadium target in a 13%/87% oxygen and argon atmosphere, with identical 17 min deposition time and 200 W plasma power. As-deposited films were amorphous. Crystallization was triggered through a 1 h long thermal annealing in an argon atmosphere, yielding polycrystalline films. As highlighted in previous works,[39,40] increasing the annealing temperature typically yields larger grains, thanks to the increase of species diffusion and boundary migration rates. Oxygen concentration during the sputtering step was also identified as a parameter having an influence on grain size, but to a smaller extent, and hence was not kept as a tuning parameter (Figure S1). The films were thus respectively annealed at 500 °C (650 °C), yielding grains with a mean size of 32 nm (210 nm) and 8 nm (77 nm) standard deviation. These parameters were extracted through SEM top view pictures and image processing (Figure 2a,b). The grain structure is also impacted by the annealing temperature (see SEM cross sections in Figure 2e,f): in the first film, the small grains tend to stack up closely across the layer thickness, while in the large-grain film, crystallite widths span across the full film thickness. The films' oxidation states were assessed through Raman spectroscopy (Figure S2): all observed peaks could be attributed to the VO_2 stoichiometry.[41] We performed X-ray diffraction (XRD) (Figure S3) to further assess the films' stoichiometry and crystallinity. Both showed similar spectra: three peaks related to the vanadium oxide layer were identified. The first corresponds to the VO_2 (011) peak, hinting that both films have a preferential (011) crystalline orientation. The other peaks could correspond to three vanadium oxide phases (discussed in Figure S3), whose signatures were absent in the Raman spectra. These XRD signatures are, however, present in both films, whose difference in transition properties will be discussed further. To that end, two-terminal microresistors were fabricated by depositing Ni/Au bilayer electrodes (5 nm/150 nm) through e-beam evaporation, patterned through lift-off. Since the VO_2 layer is not patterned, the microresistor channel area is solely determined by electrode dimensions (Figure 2c,d).

To understand the impact of grain size on stochasticity, we studied the $I-V$ characteristics of two microresistors of identical channel dimensions (L = 600 nm, W = 70 μm, Figure 2c,d) fabricated from the small- and large-grain films, respectively labeled devices A0 and B0. To obtain a good estimate of the electrical parameters' distributions, we measured 300 voltage-driven cycles for each device. Measurements were performed in a 3-probe configuration using a Keysight B1500A Semiconductor Device Analyzer to extract the exact voltage drop across the microresistor. The compliance current was set to protect the device from overheating during the metallic filament formation and avoid damages to the crystalline structure.[42−44] Measurements were

https://doi.org/10.1021/acs.nanolett.4c00184
Nano Lett. 2024, 24, 6201−6209

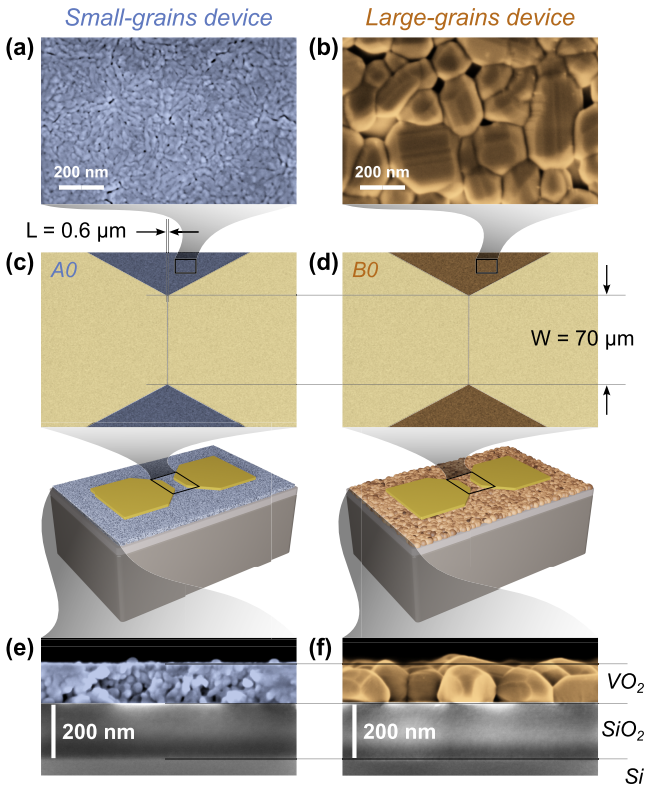

Figure 2. Two-terminal devices of identical dimensions have been fabricated from two VO_2 thin films: a small-grain film and a large-grain film (respectively in purple and orange, artificial colors). (a,b) Top views of these films imaged through SEM with identical magnification, showing a 10-fold difference in grain size (from ∼32 to ∼210 nm). (c,d) Devices labeled A0 and B0 with identical channel dimensions of L = 0.6 μm, W = 70 μm. The length is defined in the direction of the current. (e,f) Device cross sections imaged through SEM, showing that despite having an identical thickness, the VO_2 films have drastically different grain structures.

performed on a temperature-controlled chuck at 35 °C to ensure that the device did not follow room-temperature fluctuations during measurements. We start by investigating the distribution of the insulator-to-metal threshold voltage V_{IMT}, as it is a key parameter in most of the applications cited above. Results are detailed in Figure 3.

A first difference between the two devices is a much lower insulating resistance of the small-grain device (A0) compared to the large-grain one (B0), and its IMT taking place at a lower threshold voltage V_{IMT} and higher current levels. In consequence, we set different current compliances for the two devices. To investigate the cause of this resistance difference, we characterized the resistivity versus temperature hysteresis of both films (Figure S4). In addition to a smaller OFF-state resistivity, the small-grain film shows a smaller transition temperature T_{IMT} and OFF/ON resistivity ratios and a larger hysteresis width. Several works have observed such effects in correlation with grain size reduction.[45,46] They attributed them to the higher concentration of defects such as oxygen vacancies, correlated to the higher grain boundary density. Indeed, oxygen vacancies and defects have been shown to concentrate at grain boundaries.[47,48] Oxygen vacancies are often correlated to a suboxidized state of the films ($VO_{2-\delta}$) and have a an impact on the film hysteresis similar to that observed in this work.[49−52] They locally reduce the VO_2 bandgap[50] and can act as electron donors,[52] contributing to the reduction in resistivity; they also contribute to the destabilization of the monoclinic state and increase the metallicity proportion in the film,[50] reducing T_{IMT}. We thus present the hypothesis that the small-grain film could correspond to an oxygen-deficient $VO_{2-\delta}$ stoichiometry with the presence of metallic VO_2 states and increased defect concentration, possibly related to oxygen vacancies. The small-grain film also shows a smaller metallic state resistivity compared to the large-grain film, which has not been reported as a common effect of oxygen vacancies. This could be due to the larger porosity and presence of "voids" between grains in the large-grain film[53] (Figure 2b,f). As the two samples have identical (011) preferential crystalline orientation (deduced from their XRD spectra), their difference in resistivity is less likely to be related to anisotropic conductivity present in VO_2 single crystals.[54]

The second difference is that the large-grain device shows larger cycle-to-cycle V_{IMT} variability, confirming our hypothesis that larger stochastic behavior would be observed with a crystallite size getting closer to the device channel length. Threshold voltages have been extracted over 300 cycles and their distribution fitted (Figure 3g,h) after removal of a small drift over time (∼0.001%/cycle, obtained from linear regression). The difference in stochasticity is observed through two features. First, the type of distribution is purely Gaussian in the case of the small-grain device, while the large-grain device shows a mixture of two Gaussians. Second, the widths of these Gaussians, which we study through their standard deviations σ_{VIMT} (in millivolts) and coefficients of variation CV_{VIMT} (standard deviation normalized by the mean, in percentage of the mean). One notes an 18-fold ratio in σ_{VIMT} and 8-fold ratio in CV_{VIMT} when comparing the small-grain and large-grain device (taking the Gaussian with smallest width for the latter). The stochastic behavior scaling is thus true from both an absolute and relative perspective.

To go further, we also investigated how the distributions of the threshold voltages would evolve with the microresistor channel length, as shown in Figure 4. We extracted V_{IMT} values from 300 measured cycles in devices of varying channel length, fabricated from both the small-grain film (devices labeled A1−A4, see Figure 4a) and the large-grain film (devices labeled B1−B3, see Figure 4b). It is noteworthy that for small-grain devices, the channel width changed from 70 to 6 μm compared to the device studied in Figure 3a. The V_{IMT} distributions of these small-grain devices with reduced channel width and length also appear to be Gaussian mixtures. The stochastic behavior magnitude tends to decrease with increased channel length, providing a second lever to tune intrinsic stochasticity in VO_2 microresistors. Once again, this stochasticity reduction manifests itself through two distinct aspects: (1) the Gaussian mixtures observed for devices of small channel length tend to fuse into single-Gaussian distributions, and (2) the coefficients of variation of the individual Gaussians are reduced, as channel length increases. In all cases, the CV_{VIMT} orders of magnitude are similar to the previous case (see Figure 3e,f) and maintain an ∼10 ratio between the large- and small-grain devices.

We separately investigate the physical causes for these two aspects of our observations, starting with the reduction in standard deviation/coefficient of variation with reduced grain size and increased channel length. The percolation process leading to the creation of a metallic filament during voltage-triggered IMT has been shown to nucleate from "hot spots"[5,6,37] where Joule heating/electrical effects are of higher

https://doi.org/10.1021/acs.nanolett.4c00184
Nano Lett. 2024, 24, 6201−6209

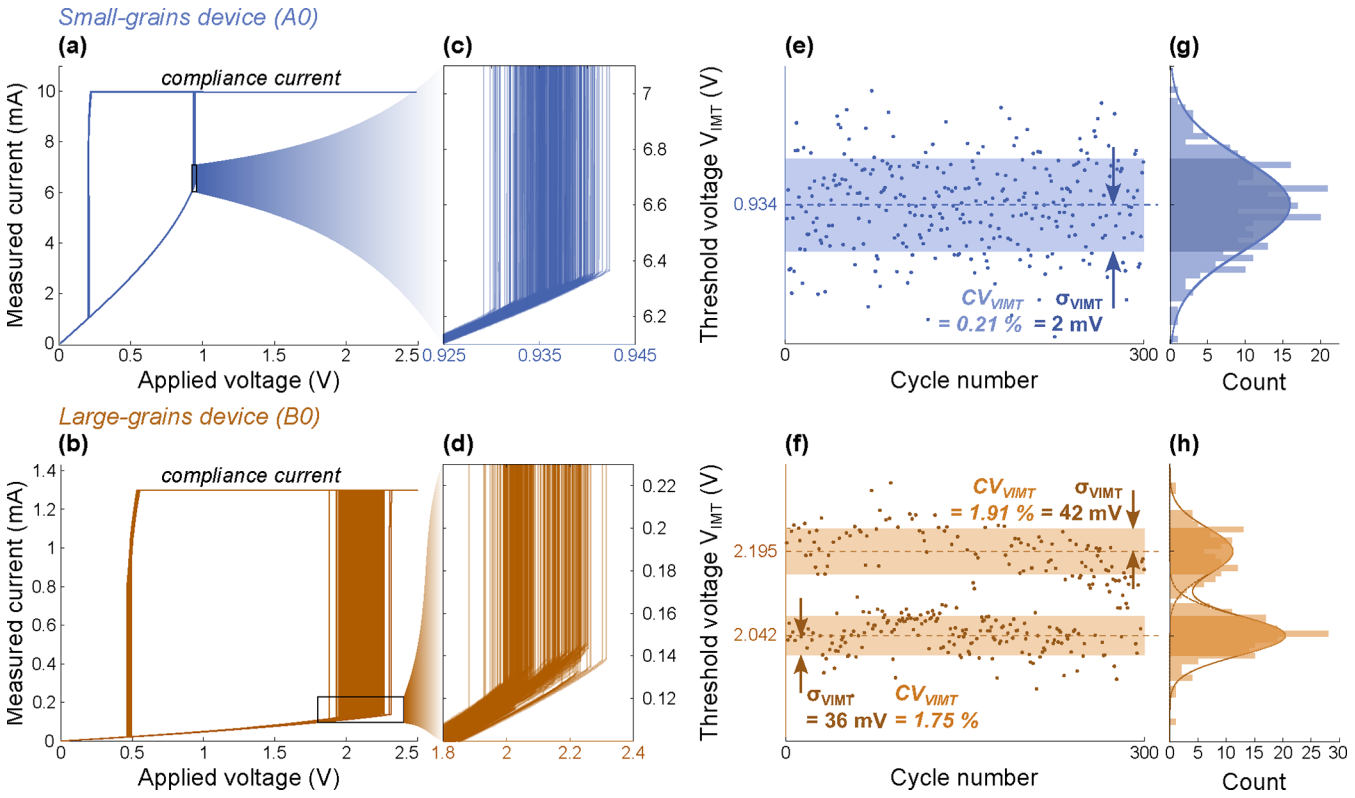

Figure 3. (a,b) Voltage-driven $I-V$ characteristics of the small-grain device (A0) and the large-grain device (B0) of identical dimensions (L = 600 nm, W = 70 μm), measured over 300 cycles. (c,d) Close-up views on the cycle-to-cycle variation in insulator-to-metal threshold voltage V_{IMT}. The larger variations in the case of device B0 are visible when comparing the colored x-axis of the two figures. (e,f) Extraction of V_{IMT} for each cycle, after drift removal. (g,h) Fit to Gaussian and Gaussian mixture distributions, respectively, for the small-grain and large-grain devices. Standard deviations σ_{VIMT} and means μ_{VIMT} are indicated, as well as the coefficients of variation CV_{VIMT}.

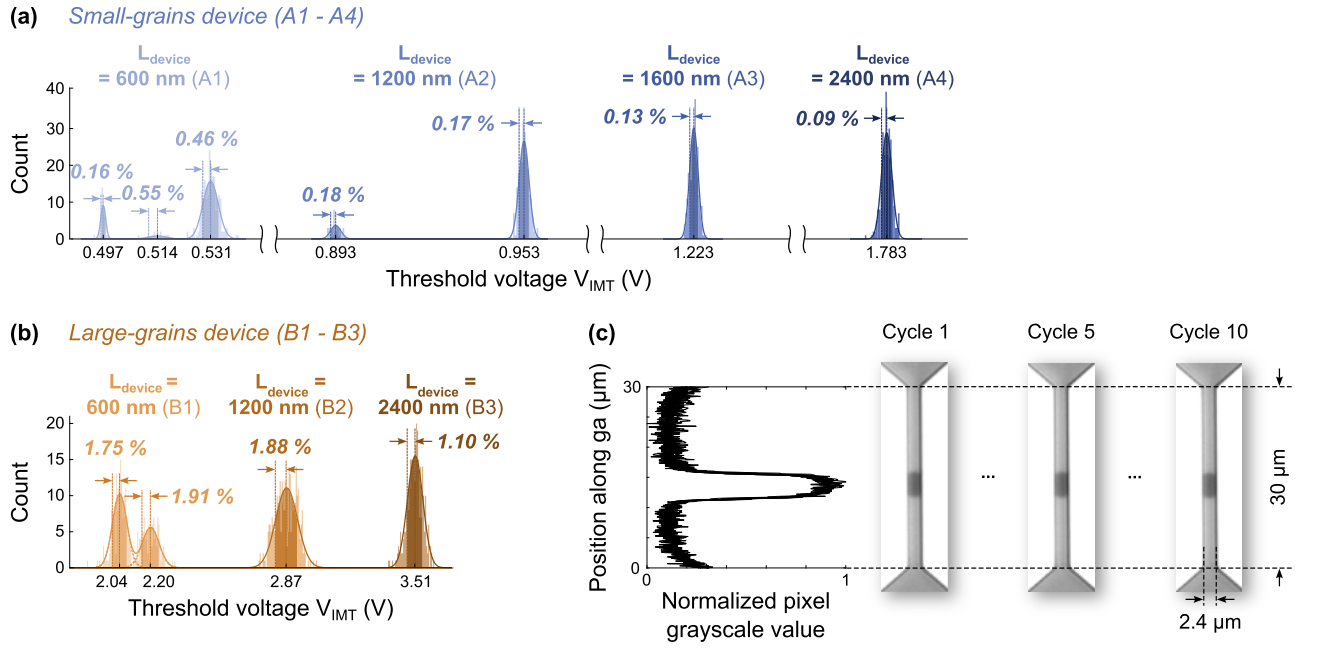

Figure 4. Impact of the VO_2 devices' channel length on their threshold voltage distributions. (a) Small-grain devices, for channel lengths of 600 (A1), 1200 (A2), 1600 (A3), and 2400 nm (A4). The channel width is 6 μm in all cases. (b) Large-grain devices, for channel lengths of 600 (B1), 1200 (B2), and 2400 nm (B3). The channel width is 70 μm in all cases. The mean and coefficient of variation are displayed for each individual Gaussian. (c) High-resolution microscopy imaging of the metallic filament across 10 cycles in a small-grain device with a 2.4 μm long channel. The plot shows normalized pixel grayscale values extracted along the channel width over 10 cycles.

intensity, and thus transition first. Once this group of crystallites has transitioned, the voltage drop redistributes across their neighbors which transition in their turn, triggering the metallic filament. We hypothesize that V_{IMT} values

https://doi.org/10.1021/acs.nanolett.4c00184
Nano Lett. 2024, 24, 6201−6209

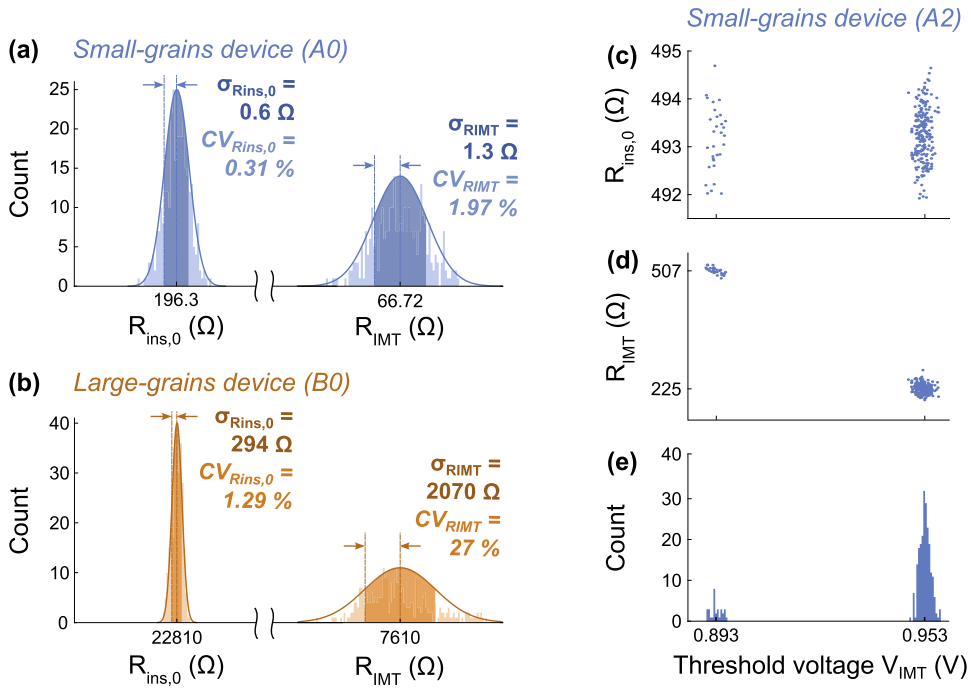

Figure 5. Distributions of the device insulating resistances close to zero bias ($R_{ins,0}$) and right before the insulator-to-metal transition (R_{IMT}), for small-grain device A0 (a) and large-grain device B0 (b) of identical dimensions (L = 600 nm, W = 70 μm). (c–e) Investigation of these two parameters for device A2, one of the devices showing a multimodal threshold voltage distribution (e). (c,d) Scatter plots of $R_{ins,0}$ and R_{IMT}, respectively, against V_{IMT}.

belonging to the same Gaussian correspond to closely located hot spots, yielding filaments in similar positions. Indeed, recent work showed that localized, ion-beam-induced defects reduced the IMT cycle-to-cycle stochasticity by defining the filament percolation hot spot.[55] To further support our claim, we imaged filaments in individual devices across several cycles using a Microsanj optical microscope, acquiring images at a wavelength of 530 nm wavelength. Results show that for devices with larger channel width (those with single-Gaussian V_{IMT} distributions), the filament always forms at the same location. Results for one of these devices are shown in Figure 4c, and the analysis has been repeated for other devices with single-Gaussian V_{IMT} distributions (Figure S5), showing that filament width is relatively constant with channel width. Although the filament always nucleates from closely localized hot spots, slight alterations of the grains' resistances from cycle to cycle could affect the initial percolation path, yielding variations in V_{IMT}. As stated earlier, experimental observations possibly explaining these variations include persistent metallic domains,[35] or changes in grains crystalline orientation,[38] both involving grains in the area of the previous cycle metallic filament. In particular, the presence of residual metallic domains has been shown to facilitate filament retriggering at the same location from cycle to cycle.[37] In both cases, as these variations involve individual grains, one expects them to have less impact on the IMT bias point if the percolation path involves a larger number of grains or if these grains are more uniform. In relation to that, we do show that the small-grain film has a smaller grain size standard deviation. Regarding uniformity, low cycle-to-cycle variability was recently reported[13] in VO_2 microresistor threshold voltages (σ_{VIMT} and CV_{VIMT} of 9.4 mV and 0.71%) and was attributed to the epitaxial nature of the VO_2 film yielding highly uniform crystallites. However, epitaxial growth requires non-CMOS-compatible substrates, such as Al_2O_3. In the case of our small-grain device A0 whose film was grown on Si/SiO_2 substrates, we observe both smaller σ_{VIMT} and CV_{VIMT} (2 mV and 0.21%), which shows that epitaxial growth might not be necessary to minimize cycle-to-cycle variations.

The grain size variation comes with differences in the films' material and electrical properties, which could also explain the stochasticity difference between the resulting devices. First, the large-grain film shows a sharper transition and a higher OFF/ON resistivity ratio. In this case, filament formation could be triggered from a smaller number of seed grains, as the "percolation effect" (applied voltage redistribution across the seed grains' neighbors, precipitating the filament creation[6]) could be stronger. This would imply stronger stochasticity in large-grain devices, consistent with our hypothesis. Second, the possible higher proportion of rutile VO_2 within the small-grain film insulating state,[50] and the possible presence of another vanadium oxide phase (hinted by XRD measurements), could impact filament formation. Third, residual stresses and strain (known to have large impacts on the IMT[33,34]) could be present with larger inhomogeneity in the large-grain film. In addition to these differences, dynamic effects related to the decay of persistent metallic islands could play a role. In our study, the high-resolution measurement of a single cycle lasts for about 10^2 s, while reported time scales for long-lasting metallic islands range from 10^{-2} [35] to 10^2 s.[37] Metallic islands are also more concentrated at temperatures closer to T_{IMT}.[35] It is thus possible that small-grain devices, which have lower T_{IMT}, contain more long-lasting metallic domains, impacting stochasticity. However, the strongest argument hinting at stochasticity being correlated to the grain number in the channel is its dependence on device length. This effect is smaller for large grains: in this case, there is a smaller number

https://doi.org/10.1021/acs.nanolett.4c00184
Nano Lett. 2024, 24, 6201−6209

of "possible seed grain locations" along the channel length axis, which could explain this difference.

Let us now investigate the possible causes for the multimodal Gaussian V_{IMT} distributions. These could correspond to distinct percolation hot spots and resulting filament locations. To our knowledge, multimodal V_{IMT} distributions have not been analyzed in VO_2 literature and have been solely observed once in VO_2 oscillators[11] with no proposed explanatory hypothesis. Our optical microscopy imaging equipment resolution did not allow us to image the filament in the devices showing multimodal V_{IMT} distributions (due to their small channel length). However, a previous work[56] studied filament localization after voltage-triggered IMT upon thermal cycling and found that while the filament always formed at the same spot in devices of larger channel length, its location was rather stochastic in devices of smaller channel length. The authors attributed this to the higher electric field arising across channels of shorter devices, triggering a purely electrical, field-induced transition. Such a transition takes place when carrier density locally reaches a critical threshold, as recently observed in VO_2 nanowires.[57] Since field-induced carrier generation is an inherently stochastic process, it could happen in any individual grain of the channel and thus trigger filament formation at different locations. Indeed, the probability of a given grain to undergo field-induced IMT increases exponentially with the local voltage drop across this grain.[4] As device distributions show a finite number of Gaussians, we could argue that there could be preferential sites for field-induced nucleation.

So far, most works that studied stochasticity in VO_2 focused on cycle-to-cycle variations in the threshold voltage V_{IMT}.[10,11,13,26,35] In this work, we also studied variations in the insulating state resistance. The importance of taking R_{ins} variations into account has recently been highlighted in the context of VO_2 spiking sensors, showing that they contribute to spike rate stochasticity with the same proportion as V_{IMT} variations.[12] To perform this study, we distinguish the device resistance close to zero bias $R_{ins,0}$ from the resistance R_{IMT} just before the IMT (Figure 1b). Indeed, the OFF-state device resistance decreases with Joule heating, as VO_2 resistivity is temperature dependent in its insulating phase. Figure 5a,b compares the distributions of these two resistances for the small-grain device A0 and large-grain device B0 of identical dimensions. A full comparison of σ and CV values for the distributions of $R_{ins,0}$, R_{IMT} and V_{IMT} is available in Figure S6. Once again, the large-grain device shows larger cycle-to-cycle variations in the two studied resistances, from both an absolute ($\sigma_{Rins,0}$ and σ_{RIMT}) and relative ($CV_{Rins,0}$ and CV_{RIMT}) perspective. Intrestingly, the coefficient of variation of the insulating resistance is much larger close to the IMT point than around zero bias. This could hint that the previously mentioned small variations in the resistances of individual grains (persistent metallic islands, change in crystalline orientation) are amplified when approaching transition. Indeed, prior to IMT, the resistance of a given grain in the channel follows a decreasing exponential temperature-dependent law.[4]

More interestingly, studying the relationship between $R_{ins,0}$, R_{IMT} and V_{IMT} gives us insight on the causes behind bimodal V_{IMT} distributions. We perform this study for device A2, one of the small-grain devices with bimodal behavior, using scatter plots between its $R_{ins,0}$ and V_{IMT} values (Figure 5c) as well as its R_{IMT} and V_{IMT} values (Figure 5d). The goal is to see whether bimodal distributions are also observed in these two parameters: while it is not the case for the resistance close to zero bias $R_{ins,0}$, for R_{IMT}, two clusters corresponding to the V_{IMT} modes are clearly visible (Figure 5c,d). The resistance just before IMT is dominated by the resistance of the zone near the hot spot, as it will be less resistive and concentrate current flow. These clusters hint that the two threshold voltages could correspond to distinct hot spots in the channel, while individual variations inside one cluster could be related to changes in grains of the same hot spot, as explained earlier. Such an observation gives further evidence that bimodal V_{IMT} distributions could correspond to distinct filamentary paths.

In conclusion, we bring evidence that cycle-to-cycle variations in VO_2 microresistor insulating resistance and threshold voltage increase as the grain size approaches device dimensions. We prove this claim by separately studying the effects of grain size and channel length, showing that both are effective parameters to control stochasticity in absolute and relative ways. Reducing the grain size by ~10 while keeping the device width, length, and thickness constant allows the threshold voltage coefficient of variation to be reduced by ~10. Regarding device length, increasing it by a factor of 4 yields 6-fold and ~2-fold reductions of CV_{VIMT} for small- and large-grain devices, respectively. Our explanations are based on the previously studied existence of variations in individual grains during relaxation, hinting that the formation of the metallic filament will be less impacted by these variations if it involves a larger number of grains. The grain size difference is accompanied by large variations in the films' transition properties (possibly related to differences in metallicity, oxygen deficiency, and composition). This could impact filament formation and further contribute to the difference in cycle-to-cycle stochasticity. However, the device-length dependence of stochasticity provides strong evidence of its correlation to grain size. For the first time, we thus provide experimentally verified guidelines to design devices with minimized/maximized stochasticity, depending on the targeted application (greater device-to-device variability is, however, expected for large-grain devices). These conclusions could possibly hold true for resistive switching devices with filamentary transition based on other materials (V_3O_5,[58] V_2O_3,[59] NbO_2[60]). We also detail unprecedented analyses of multimodal distributions in threshold voltages for devices of small channel length. By showing the presence of clustering between the threshold voltages and insulating resistances values in such devices, we show that these modes could be attributed to distinct percolation hot spots, contributing to the current understanding of stochastic processes in VO_2 devices.

■ ASSOCIATED CONTENT

Supporting Information

The Supporting Information is available free of charge at https://pubs.acs.org/doi/10.1021/acs.nanolett.4c00184.

Additional information about the impact of oxygen concentration during sputtering step on the film grain size, the process parameters during sputtering and annealing steps, Raman and XRD characterization of the VO_2 films, resistivity versus temperature hysteresis of the two films, optical imaging of the filament in several devices, and complete comparison of the distributions of electrical parameters of small- and large-grain devices A0 and B0 (PDF)

https://doi.org/10.1021/acs.nanolett.4c00184
Nano Lett. 2024, 24, 6201−6209

AUTHOR INFORMATION

Corresponding Authors

Noémie Bidoul − *Institute for Information and Communication Technologies, Electronics and Applied Mathematics (ICTEAM), UCLouvain, Louvain-la-Neuve 1348, Belgium;* orcid.org/0000-0001-5606-7114; Email: noemie.bidoul@gmail.com

Denis Flandre − *Institute for Information and Communication Technologies, Electronics and Applied Mathematics (ICTEAM), UCLouvain, Louvain-la-Neuve 1348, Belgium*; Email: denis.flandre@gmail.com

Author

Nicolas Roisin − *Institute for Information and Communication Technologies, Electronics and Applied Mathematics (ICTEAM), UCLouvain, Louvain-la-Neuve 1348, Belgium;* orcid.org/0000-0002-4251-1648

Complete contact information is available at: https://pubs.acs.org/10.1021/acs.nanolett.4c00184

Funding

This publication was supported by the French Community of Belgium in the framework of FRIA grant no. 40015488.

Notes

The authors declare no competing financial interest.

ACKNOWLEDGMENTS

The authors thank the staff of the Winfab cleanroom and Welcome characterization lab in UCLouvain for their support, as well as Benjamin Huet, Ferran Ureña Begara, and Jean-Pierre Raskin for fruitful discussions.

REFERENCES

(1) Valmianski, I.; Wang, P. Y.; Wang, S.; Ramirez, J. G.; Guénon, S.; Schuller, I. K. Origin of the Current-Driven Breakdown in Vanadium Oxides: Thermal versus Electronic. *Phys. Rev. B* **2018**, *98* (19), No. 195144.

(2) Gopalakrishnan, G.; Ruzmetov, D.; Ramanathan, S. On the Triggering Mechanism for the Metal−Insulator Transition in Thin Film VO2 Devices: Electric Field versus Thermal Effects. *J. Mater. Sci.* **2009**, *44* (19), 5345−5353.

(3) Zimmers, A.; Aigouy, L.; Mortier, M.; Sharoni, A.; Wang, S.; West, K. G.; Ramirez, J. G.; Schuller, I. K. Role of Thermal Heating on the Voltage Induced Insulator-Metal Transition in VO2. *Phys. Rev. Lett.* **2013**, *110* (5), No. 056601.

(4) Madan, H.; Jerry, M.; Pogrebnyakov, A.; Mayer, T.; Datta, S. Quantitative Mapping of Phase Coexistence in Mott-Peierls Insulator during Electronic and Thermally Driven Phase Transition. *ACS Nano* **2015**, *9* (2), 2009.

(5) del Valle, J.; Vargas, N. M.; Rocco, R.; Salev, P.; Kalcheim, Y.; Lapa, P. N.; Adda, C.; Lee, M.-H.; Wang, P. Y.; Fratino, L.; Rozenberg, M. J.; Schuller, I. K. Spatiotemporal Characterization of the Field-Induced Insulator-to-Metal Transition. *Science* **2021**, *373* (6557), 907−911.

(6) Stoliar, P.; Cario, L.; Janod, E.; Corraze, B.; Guillot-Deudon, C.; Salmon-Bourmand, S.; Guiot, V.; Tranchant, J.; Rozenberg, M. Universal Electric-Field-Driven Resistive Transition in Narrow-Gap Mott Insulators. *Adv. Mater.* **2013**, *25* (23), 3222−3226.

(7) Yi, W.; Tsang, K. K.; Lam, S. K.; Bai, X.; Crowell, J. A.; Flores, E. A. Biological Plausibility and Stochasticity in Scalable VO2 Active Memristor Neurons. *Nat. Commun.* **2018**, *9*, 4661.

(8) Yuan, R.; Tiw, P. J.; Cai, L.; Yang, Z.; Liu, C.; Zhang, T.; Ge, C.; Huang, R.; Yang, Y. A Neuromorphic Physiological Signal Processing System Based on VO2 Memristor for Next-Generation Human-Machine Interface. *Nat. Commun.* **2023**, *14* (1), 3695.

(9) Belyaev, M.; Velichko, A. A Spiking Neural Network Based on the Model of VO2—Neuron. *Electronics* **2019**, *8*, 1065.

(10) Parihar, A.; Jerry, M.; Datta, S.; Raychowdhury, A. Stochastic IMT (Insulator-Metal-Transition) Neurons: An Interplay of Thermal and Threshold Noise at Bifurcation. *Front. Neurosci.* **2018**, *12*, 210.

(11) Qaderi, F.; Rosca, T.; Burla, M.; Leuthold, J.; Flandre, D.; Ionescu, A. M. Millimeter-Wave to near-Terahertz Sensors Based on Reversible Insulator-to-Metal Transition in VO2. *Commun. Mater.* **2023**, *4* (1), 1−12.

(12) Bidoul, N.; Rosca, T.; Ionescu, A. M.; Flandre, D. Static and Dynamic Stochastic Analysis of a Temperature-Sensitive VO $_2$ Spiking Neuron. In *ESSDERC 2023 - IEEE 53rd European Solid-State Device Research Conference (ESSDERC)*; IEEE: 2023; pp 81−84. DOI: 10.1109/ESSDERC59256.2023.10268509.

(13) Yuan, R.; Duan, Q.; Tiw, P. J.; Li, G.; Xiao, Z.; Jing, Z.; Yang, K.; Liu, C.; Ge, C.; Huang, R.; Yang, Y. A Calibratable Sensory Neuron Based on Epitaxial VO2 for Spike-Based Neuromorphic Multisensory System. *Nat. Commun.* **2022**, *13* (1), 3973.

(14) Han, C. Y.; Han, Z. R.; Fang, S. L.; Fan, S. Q.; Yin, J. Q.; Liu, W. H.; Li, X.; Yang, S. Q.; Zhang, G. H.; Wang, X. L.; Geng, L. Characterization and Modelling of Flexible VO2 Mott Memristor for the Artificial Spiking Warm Receptor. *Adv. Mater. Interfaces* **2022**, *9* (19), No. 2200394.

(15) Fang, S. L.; Han, C. Y.; Liu, W.; Han, Z. R.; Ma, B.; Cui, Y. L.; Fan, S. Q.; Li, X.; Wang, X. L.; Zhang, G. H.; Yin, J. Q.; Huang, X. D.; Geng, L. A Bioinspired Flexible Artificial Mechanoreceptor Based on VO2 Insulator-Metal Transition Memristor. *J. Alloys Compd.* **2022**, *911*, No. 165096.

(16) Rosca, T.; Qaderi, F.; Ionescu, A. M. High Tuning Range Spiking 1R-1T VO2 Voltage-Controlled Oscillator for Integrated RF and Optical Sensing. In *ESSCIRC 2021 - IEEE 47th European Solid State Circuits Conference (ESSCIRC)*; IEEE: 2021; pp 183−186. .

(17) Deng, X.; Wang, S.-Q.; Liu, Y.-X.; Zhong, N.; He, Y.-H.; Peng, H.; Xiang, P.-H.; Duan, C.-G. A Flexible Mott Synaptic Transistor for Nociceptor Simulation and Neuromorphic Computing. *Adv. Funct. Mater.* **2021**, *31* (23), No. 2101099.

(18) Wang, Y.; Su, C.; Zheng, Y.; Zhou, K.; Wen, Z.; Fu, Y.; Wang, Q.; He, D. High Consistency VO2 Memristor for Artificial Auditory Neuron. *Microelectron. Eng.* **2023**, *282*, No. 112101.

(19) Frenkel, C. Sparsity Provides a Competitive Advantage. *Nat. Mach. Intell.* **2021**, *3* (9), 742−743.

(20) Maass, W. Networks of Spiking Neurons: The Third Generation of Neural Network Models. *Neural Netw.* **1997**, *10* (9), 1659−1671.

(21) Ying, J.; Min, F.; Wang, G. Neuromorphic Behaviors of VO2 Memristor-Based Neurons. *Chaos Solitons Fractals* **2023**, *175*, No. 114058.

(22) Basak, S.; Sun, Y.; Banguero, M. A.; Salev, P.; Schuller, I. K.; Aigouy, L.; Carlson, E. W.; Zimmers, A. Spatially Distributed Ramp Reversal Memory in VO2. *Adv. Electron. Mater.* **2023**, *9* (10), No. 2300085.

(23) Samizadeh Nikoo, M.; Soleimanzadeh, R.; Krammer, A.; Migliato Marega, G.; Park, Y.; Son, J.; Schueler, A.; Kis, A.; Moll, P. J. W.; Matioli, E. Electrical Control of Glass-like Dynamics in Vanadium Dioxide for Data Storage and Processing. *Nat. Electron.* **2022**, *5* (9), 596−603.

(24) Li, G.; Xie, D.; Zhong, H.; Zhang, Z.; Fu, X.; Zhou, Q.; Li, Q.; Ni, H.; Wang, J.; Guo, E.; He, M.; Wang, C.; Yang, G.; Jin, K.; Ge, C. Photo-Induced Non-Volatile VO2 Phase Transition for Neuromorphic Ultraviolet Sensors. *Nat. Commun.* **2022**, *13* (1), 1729.

(25) Shabalin, A. G.; del Valle, J.; Hua, N.; Cherukara, M. J.; Holt, M. V.; Schuller, I. K.; Shpyrko, O. G. Nanoscale Imaging and Control of Volatile and Non-Volatile Resistive Switching in VO2. *Small* **2020**, *16* (50), No. 2005439.

(26) Jerry, M.; Ni, K.; Parihar, A.; Raychowdhury, A.; Datta, S. Stochastic Insulator-to-Metal Phase Transition-Based True Random Number Generator. *IEEE Electron Device Lett.* **2018**, *39* (1), 139−142.

(27) del Valle, J.; Salev, P.; Gariglio, S.; Kalcheim, Y.; Schuller, I. K.; Triscone, J.-M. Generation of Tunable Stochastic Sequences Using the Insulator−Metal Transition. *Nano Lett.* **2022**, *22* (3), 1251−1256.
(28) Deng, S.; Park, T. J.; Yu, H.; Saha, A.; Islam, A. N. M. N.; Wang, Q.; Sengupta, A.; Ramanathan, S. Hydrogenated VO_2 Bits for Probabilistic Computing. *IEEE Electron Device Lett.* **2023**, *44* (10), 1776−1779.
(29) Bhar, B.; Khanna, A.; Parihar, A.; Datta, S.; Raychowdhury, A. Stochastic Resonance in Insulator-Metal-Transition Systems. *Sci. Rep.* **2020**, *10* (1), 5549.
(30) Qiu, E.; Salev, P.; Torres, F.; Navarro, H.; Dynes, R. C.; Schuller, I. K. Stochastic Transition in Synchronized Spiking Nanooscillators. *Proc. Natl. Acad. Sci. U.S.A.* **2023**, *120* (38), No. e2303765120.
(31) Bao, L.; Wang, Z.; Wang, B.; Liu, K.; Bai, G.; Yu, Z.; Kang, J.; Ling, Y.; Wu, L.; Chen, Q.; Niang, K.; Cai, Y.; Robertson, J.; Huang, R. Tunable Stochastic Oscillator Based on Hybrid VO2/TaOx Device for Compressed Sensing. *IEEE Electron Device Lett.* **2021**, *42*, 102−105.
(32) Zhang, K.; Wang, B.; Wang, F.; Han, Y.; Jian, X.; Zhang, H.; Wong, H. S. P. VO2-Based Selection Device for Passive Resistive Random Access Memory Application. *IEEE Electron Device Lett.* **2016**, *37* (8), 978−981.
(33) Salev, P.; Kisiel, E.; Sasaki, D.; Gunn, B.; He, W.; Feng, M.; Li, J.; Tamura, N.; Poudyal, I.; Islam, Z.; Takamura, Y.; Frano, A.; Schuller, I. K. Local Strain Inhomogeneities during the Electrical Triggering of a Metal-Insulator Transition Revealed by the x-Ray Microscopy. *arXiv (Condensed matter, Materials Science)*. 2023. DOI: 10.48550/arXiv.2310.07001 (accessed on 2024-01-08).
(34) Arata, Y.; Nishinaka, H.; Takeda, M.; Kanegae, K.; Yoshimoto, M. Strain-Induced Modulation of Resistive Switching Temperature in Epitaxial VO2 Thin Films on Flexible Synthetic Mica. *ACS Omega* **2022**, *7* (45), 41768−41774.
(35) del Valle, J.; Salev, P.; Tesler, F.; Vargas, N. M.; Kalcheim, Y.; Wang, P.; Trastoy, J.; Lee, M.-H.; Kassabian, G.; Ramírez, J. G.; Rozenberg, M. J.; Schuller, I. K. Subthreshold Firing in Mott Nanodevices. *Nature* **2019**, *569* (7756), 388−392.
(36) Ramírez, J.-G.; Sharoni, A.; Dubi, Y.; Gómez, M. E.; Schuller, I. K. First-Order Reversal Curve Measurements of the Metal-Insulator Transition in VO2: Signatures of Persistent Metallic Domains. *Phys. Rev. B* **2009**, *79* (23), No. 235110.
(37) Kisiel, E.; Salev, P.; Poudyal, I.; Baptista, F.; Rodolakis, F.; Zhang, Z.; Shpyrko, O.; Schuller, I. K.; Islam, Z.; Frano, A. High-Resolution Full-Field Structural Microscopy of the Voltage Induced Filament Formation in Neuromorphic Devices. *arXiv (Physics, Applied Physics)*. 2023. DOI: 10.48550/arXiv.2309.15712 (accessed on 2024-01-05).
(38) Cheng, S.; Lee, M.-H.; Tran, R.; Shi, Y.; Li, X.; Navarro, H.; Adda, C.; Meng, Q.; Chen, L.-Q.; Dynes, R. C.; Ong, S. P.; Schuller, I. K.; Zhu, Y. Inherent Stochasticity during Insulator−Metal Transition in VO_2. *Proc. Natl. Acad. Sci. U.S.A.* **2021**, *118* (37), No. e2105895118.
(39) Liu, D.; Yang, P.; Zhang, Y.; Chen, Y.; Dai, H.; Li, T.; Xue, R.; Chen, J.; Su, Y.; Chen, Z. Effects of Microdefects and Grain Size on the Phase Transition Properties of Nano-VO2(M). *J. Solid State Chem.* **2020**, *288*, No. 121450.
(40) Liu, Y.; Liu, J.; Li, Y.; Wang, D.; Ren, L.; Zou, K. Effect of Annealing Temperature on the Structure and Properties of Vanadium Oxide Films. *Opt. Mater. Express* **2016**, *6* (5), 1552.
(41) Shvets, P.; Dikaya, O.; Maksimova, K.; Goikhman, A. A Review of Raman Spectroscopy of Vanadium Oxides. *J. Raman Spectrosc.* **2019**, *50* (8), 1226−1244.
(42) Shabalin, A. G.; del Valle, J.; Charnukha, A.; Hua, N.; Holt, M. V.; Basov, D. N.; Schuller, I. K.; Shpyrko, O. G. Nanoimaging of Electrical Failure in VO2 Resistive-Switching Nanodevices. *ACS Appl. Electron. Mater.* **2020**, *2* (8), 2357−2362.
(43) Jeong, J.; Yong, Z.; Joushaghani, A.; Tsukernik, A.; Paradis, S.; Alain, D.; Poon, J. K. S. Current Induced Polycrystalline-to-Crystalline Transformation in Vanadium Dioxide Nanowires. *Sci. Rep.* **2016**, *6* (1), No. 37296.
(44) Lin, J.; Alam, K.; Ocola, L.; Zhang, Z.; Datta, S.; Ramanathan, S.; Guha, S. Physics and Technology of Electronic Insulator-to-Metal Transition (E-IMT) for Record High on/off Ratio and Low Voltage in Device Applications. In *2017 IEEE International Electron Devices Meeting (IEDM)*; IEEE: 2017; pp 23.4.1−23.4.4. .
(45) Niang, K. M.; Bai, G.; Lu, H.; Robertson, J. Microstructure Scaling of Metal−Insulator Transition Properties of VO2 Films. *Appl. Phys. Lett.* **2021**, *118* (12), No. 121901.
(46) Ainabayev, A.; Mullarkey, D.; Walls, B.; Caffrey, D.; Zhussupbekov, K.; Zhussupbekova, A.; Ilhan, C.; Kaisha, A.; Biswas, P.; Tikhonov, A.; Murtagh, O.; Shvets, I. Epitaxial Grown VO2 with Suppressed Hysteresis and Low Room Temperature Resistivity for High-Performance Thermal Sensor Applications. *ACS Appl. Nano Mater.* **2023**, *6* (4), 2917−2927.
(47) Lu, W.; Wong, L.-M.; Wang, S.; Zeng, K. Local Phenomena at Grain Boundaries: An Alternative Approach to Grasp the Role of Oxygen Vacancies in Metallization of VO2. *J. Mater.* **2018**, *4* (4), 360−367.
(48) Jian, J.; Zhang, W.; Jacob, C.; Chen, A.; Wang, H.; Huang, J.; Wang, H. Roles of Grain Boundaries on the Semiconductor to Metal Phase Transition of VO2 Thin Films. *Appl. Phys. Lett.* **2015**, *107* (10), No. 102105.
(49) Lu, Q.; Sohn, C.; Hu, G.; Gao, X.; Chisholm, M. F.; Kylänpää, I.; Krogel, J. T.; Kent, P. R. C.; Heinonen, O.; Ganesh, P.; Lee, H. N. Metal−Insulator Transition Tuned by Oxygen Vacancy Migration across TiO2/VO2 Interface. *Sci. Rep.* **2020**, *10* (1), No. 18554.
(50) Zhang, Z.; Zuo, F.; Wan, C.; Dutta, A.; Kim, J.; Rensberg, J.; Nawrodt, R.; Park, H. H.; Larrabee, T. J.; Guan, X.; Zhou, Y.; Prokes, S. M.; Ronning, C.; Shalaev, V. M.; Boltasseva, A.; Kats, M. A.; Ramanathan, S. Evolution of Metallicity in Vanadium Dioxide by Creation of Oxygen Vacancies. *Phys. Rev. Appl.* **2017**, *7* (3), No. 034008.
(51) Zhang, J.; Zhao, Z.; Li, J.; Jin, H.; Rehman, F.; Chen, P.; Jiang, Y.; Chen, C.; Cao, M.; Zhao, Y. Evolution of Structural and Electrical Properties of Oxygen-Deficient VO2 under Low Temperature Heating Process. *ACS Appl. Mater. Interfaces* **2017**, *9* (32), 27135−27141.
(52) Jeong, J.; Aetukuri, N.; Graf, T.; Schladt, T. D.; Samant, M. G.; Parkin, S. S. P. Suppression of Metal-Insulator Transition in VO2 by Electric Field−Induced Oxygen Vacancy Formation. *Science* **2013**, *339* (6126), 1402−1405.
(53) Yu, S.; Wang, S.; Lu, M.; Zuo, L. A Metal-Insulator Transition Study of VO2 Thin Films Grown on Sapphire Substrates. *J. Appl. Phys.* **2017**, *122* (23), No. 235102.
(54) Bongers, P. F. Anisotropy of the electrical conductivity of VO2 single crystals. *Solid State Commun.* **1965**, *3* (9), 275−277.
(55) Ghazikhanian, N.; del Valle, J.; Salev, P.; El Hage, R.; Kalcheim, Y.; Adda, C.; Schuller, I. K. Resistive Switching Localization by Selective Focused Ion Beam Irradiation. *Appl. Phys. Lett.* **2023**, *123* (12), No. 123505.
(56) Yoon, J.; Lee, G.; Park, C.; Mun, B. S.; Ju, H. Investigation of Length-Dependent Characteristics of the Voltage-Induced Metal Insulator Transition in VO2 Film Devices. *Appl. Phys. Lett.* **2014**, *105* (8), No. 083503.
(57) Kalcheim, Y.; Camjayi, A.; del Valle, J.; Salev, P.; Rozenberg, M.; Schuller, I. K. Non-Thermal Resistive Switching in Mott Insulator Nanowires. *Nat. Commun.* **2020**, *11* (1), 2985.
(58) Das, S. K.; Nandi, S. K.; Marquez, C. V.; Rúa, A.; Uenuma, M.; Puyoo, E.; Nath, S. K.; Albertini, D.; Baboux, N.; Lu, T.; Liu, Y.; Haeger, T.; Heiderhoff, R.; Riedl, T.; Ratcliff, T.; Elliman, R. G. Physical Origin of Negative Differential Resistance in V3O5 and Its Application as a Solid-State Oscillator. *Adv. Mater.* **2023**, *35* (8), No. 2208477.
(59) Lange, M.; Guénon, S.; Kalcheim, Y.; Luibrand, T.; Vargas, N. M.; Schwebius, D.; Kleiner, R.; Schuller, I. K.; Koelle, D. Imaging of Electrothermal Filament Formation in a Mott Insulator. *Phys. Rev. Appl.* **2021**, *16* (5), No. 054027.

(60) Kumar, S.; Wang, Z.; Davila, N.; Kumari, N.; Norris, K. J.; Huang, X.; Strachan, J. P.; Vine, D.; Kilcoyne, A. L. D.; Nishi, Y.; Williams, R. S. Physical Origins of Current and Temperature Controlled Negative Differential Resistances in NbO2. *Nat. Commun.* **2017**, *8* (1), 658.

https://doi.org/10.1021/acs.nanolett.4c00184
Nano Lett. 2024, 24, 6201−6209